Controlled Self-Assembly of Proteins into Discrete Nanoarchitectures Templated by Gold Nanoparticles via Monovalent Interfacial Engineering

ARTICLE *in* ACS APPLIED MATERIALS & INTERFACES · MAY 2015

Impact Factor: 6.72 · DOI: 10.1021/acsami.5b02823 · Source: PubMed

5 AUTHORS, INCLUDING:

Feng Li

Wuhan Institute Of Virology

18 PUBLICATIONS **574** CITATIONS

SEE PROFILE

ACS APPLIED MATERIALS & INTERFACES

Research Article

www.acsami.org

Controlled Self-Assembly of Proteins into Discrete Nanoarchitectures Templated by Gold Nanoparticles via Monovalent Interfacial Engineering

Lingzhi Ma,[†] Feng Li,*[,‡] Ti Fang,[‡] Jianting Zhang,[†] and Qiangbin Wang*[,†]

[†]Key Laboratory of Nano-Bio Interface, Division of Nanobiomedicine and *i*-Lab, CAS Center for Excellence in Brain Science, Suzhou Institute of Nano-Tech and Nano-Bionics, Chinese Academy of Sciences, 398 Ruoshui Road, Suzhou 215123, P. R. China

[‡]State Key Laboratory of Virology, Wuhan Institute of Virology, Chinese Academy of Sciences, No. 44, Xiaohongshan, Wuhan 430071, P. R. China

Supporting Information

ABSTRACT: Designed rational assembly of proteins promises novel properties and functionalities as well as new insights into the nature of life. *De novo* design of artificial protein nanostructures has been achieved using protein subunits or peptides as building blocks. However, controlled assembly of protein nanostructures into higher-order discrete nanoarchitectures, rather than infinite arrays or aggregates, remains a challenge due to the complex or symmetric surface chemistry of protein nanostructures. Here we develop a facile strategy to control the hierarchical assembly of protein nanocages into discrete nanoarchitectures with gold nanoparticles (AuNPs) as scaffolds via rationally designing their interfacial interaction. The protein nanocage is monofunctionalized with a polyhistidine tag (Histag) on the external surface through a mixed assembly strategy, while AuNPs are modified with Ni^{2+}–NTA chelates, so that the protein nanocage can controllably assemble onto the AuNPs via the Histag–Ni^{2+} affinity. Discrete protein nanoarchitectures with tunable composition can be generated by stoichiometric control over the ratio of protein nanocage to AuNP or change of AuNP size. The methodology described here is extendable to other protein nanostructures and chemically synthesized nanomaterials, and can be borrowed by synthetic biology for biomacromolecule manipulation.

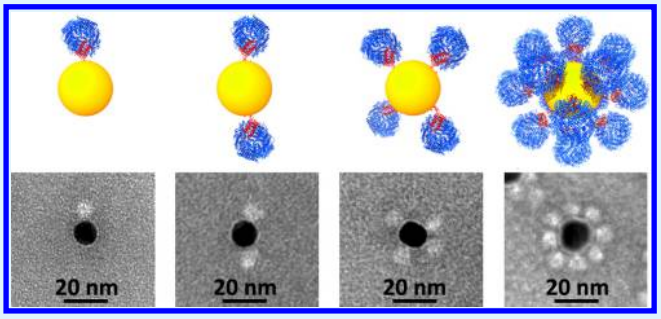

KEYWORDS: *self-assembly, protein nanostructure, discrete nanoarchitecture, gold nanoparticle, monofunctionalization*

1. INTRODUCTION

Proteins, the most versatile building blocks in nature, are responsible for structural and functional complexity of life. Self-assembly of proteins into nano- or microscale architectures, such as ATPase,[1] microtubule,[2] and bacterial microcompartment,[3] constitutes the basis of life. Designed protein assembly, which not only helps understand the nature of life but also promises novel functional materials for a wide range of applications including biomedical imaging, drug delivery, biosensors, immunotherapy, enzyme catalysis, and electronics, has attracted increasing interest in recent years.[4−11] Protein nanocages,[6,10,12−14] curved disks,[15] nanosheets,[16] nanoparticles (NPs),[7] and periodic arrays[11,17] have been assembled with protein subunits or peptides as building blocks through rational interface design. However, investigation on hierarchical assembly of these protein nanostructures into discrete nanoarchitectures, which is the next critical step in developing protein-based materials, devices, and machines, is still in its infancy. Although there have been a few attempts at assembling two-dimensional (2D) or three-dimensional (3D) arrays of protein nanocages,[4,9,18] fabrication of well-organized complicated finite architectures with protein nanostructures as building blocks remains a great challenge. The major difficulty is derived from the complex surface chemistry and structural symmetry of protein nanostructures, which cause uncontrollability in the assembly process. Here we report the organization of protein nanocages into discrete nanoarchitectures using gold NPs (AuNPs) as scaffolds through rationally engineering the protein–AuNP interfacial interaction via a simple chemical strategy.

Chemically synthesized nanomaterials, such as metal or semiconductor NPs, which are amendable for various surface functionalization,[19−21] are ideal scaffolds for templating the assembly of protein nanostructures. In this work, by taking the Dps (DNA binding protein from starved cells) nanocage from *Listeria innocua* and AuNPs as model motifs, we controllably assembled finite Dps–AuNP hybrid nanoarchitectures via a facile interfacial engineering strategy; that is, each Dps is first installed with a single polyhistidine tag (Histag) on the external surface in virtue of a mixed assembly strategy developed

Received: March 31, 2015
Accepted: May 6, 2015
Published: May 6, 2015

DOI: 10.1021/acsami.5b02823
ACS Appl. Mater. Interfaces 2015, 7, 11024−11031

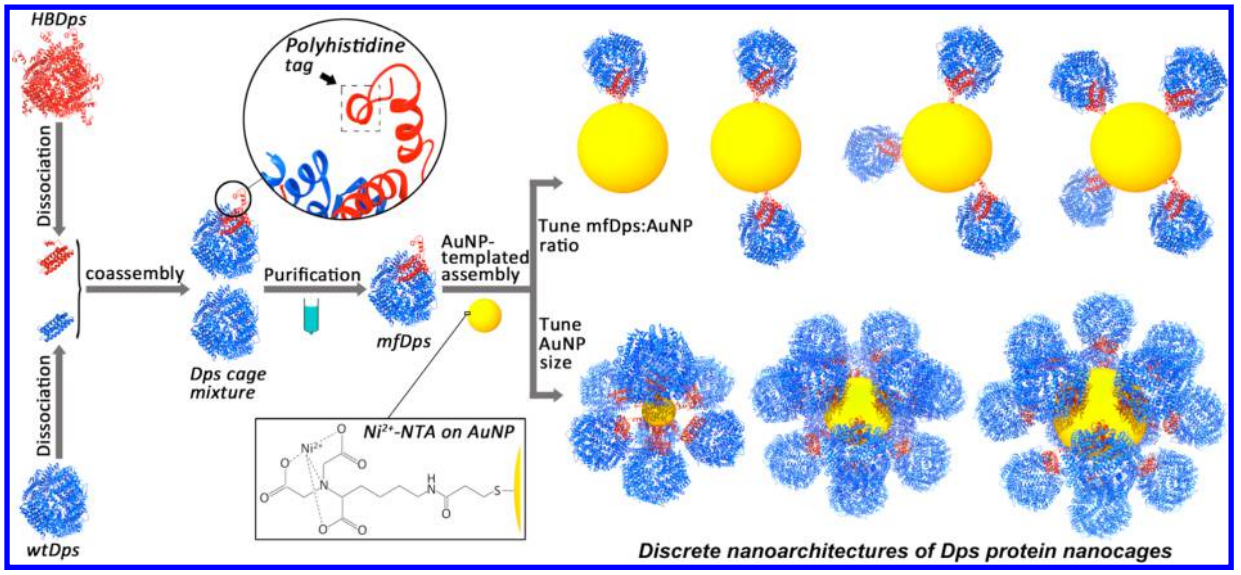

Figure 1. Schematic illustration of the AuNP-templated assembly of discrete nanoarchitectures of Dps.

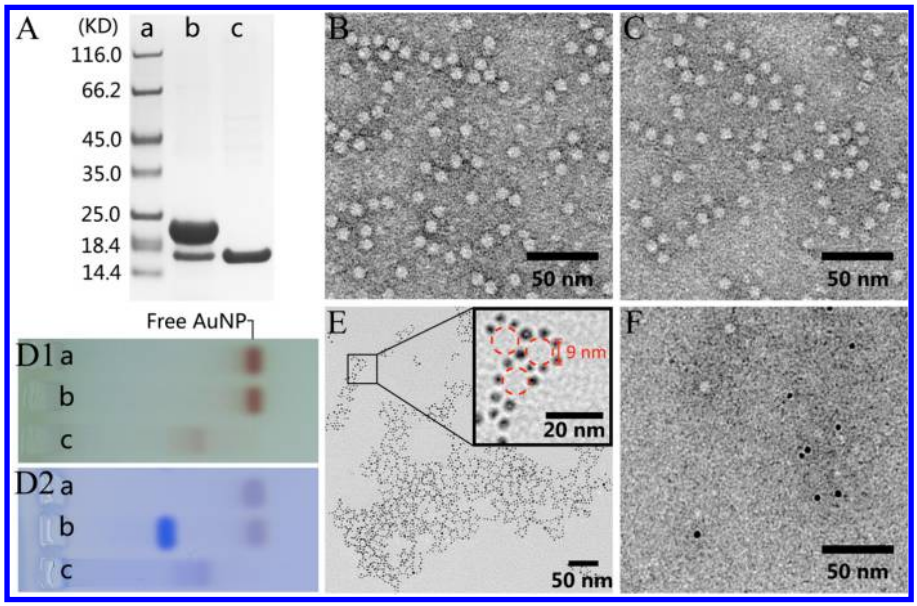

Figure 2. Characterization of wtDps and HBDps. (A) SDS-PAGE of purified Dps proteins. Lanes a–c, marker, HBDps, and wtDps, respectively. (B,C) TEM images of HBDps (B) and wtDps (C) nanocages. (D) Agarose gel (2%) electrophoresis images of Dps–AuNP mixtures before (D1) and after (D2) CBB R-250 staining. Lanes a–c, 3.5 nm Ni^{2+}–NTA–AuNPs, mixture of wtDps–AuNPs, and mixture of HBDps–AuNPs, respectively. (E,F) TEM images of HBDps–AuNP aggregates (E) and wtDps–AuNP mixture (F). Inset in part E shows an enlarged view of HBDps–AuNP aggregates. The dashed red circles 9 nm in diameter imply the presence of HBDps.

previously in our lab,[22] while the AuNP is modified with Ni^{2+} bound nitrilotriacetic acid (Ni^{2+}–NTA) using the reagent 3,3′-dithiobis[*N*-(5-amino-5-carboxypentyl) propionamide-*N*,*N*′-diacetic acid] dihydrochloride (abbreviated as Dithiobis(C2-NTA)), so that the monofunctionalized Dps (mfDps) can monovalently bind to AuNPs through the classic Ni^{2+} affinity to Histag (see Supporting Information for details). In this way, the Dps species are controllably assembled onto AuNPs, and the number of protein nanocages per AuNP is tunable by either adjusting the stoichiometry of mfDps to AuNPs or changing the size of AuNPs (Figure 1).

2. RESULTS AND DISCUSSION

Dps has a cage-like structure composed of 12 identical 18 kDa, with a 9 nm outer diameter and a 5 nm inner cavity diameter. The N terminus of the subunit is exposed on the external surface of the Dps cage.[23] The switch between cage and monomer is dictated by solution pH. Dps exists predominantly as monomer when the pH value is as low as 2.0 and assembles into a cage when the pH value is raised to 7.0.[24] Monofunctionalization of a Dps nanocage is based on coassembly of the functional and nonfunctional monomers followed by purification. Dps monomer with the N terminus fused with a Histag serves as the functional building block (HBDps), while wild-type Dps (wtDps) monomer serves as the nonfunctional one (Figure 1). WtDps and HBDps were recombinantly expressed in *E. coli*, purified, and analyzed by sodium dodecyl sulfate polyacrylamide gel electrophoresis (SDS-PAGE) (Figure 2A). It is noted that there is a band with a lower molecular weight (MW, equivalent to that of

DOI: 10.1021/acsami.5b02823
ACS Appl. Mater. Interfaces 2015, 7, 11024–11031

wtDps, 18 kDa) in the lane of the HBDps sample (predicted MW of HBDps: 21 kDa). Mass spectrometry analysis indicated that it corresponds to wtDps (Supporting Information Figure S1), which is encoded within the open reading frame of HBDps, probably translated from the second ATG codon due to ribosomal leaky scanning, and purified accompanying HBDps because of hybrid assembly. According to transmission electron microscopy (TEM) examination, HBDps forms a spheric structure like wtDps, with a diameter around 9 nm (Figure 2B,C).

To test the surface functionality in terms of their interaction with AuNPs, HBDps and wtDps were individually incubated with AuNPs of 3.5 nm in diameter which were functionalized by the Ni^{2+}–NTA chelates. Agarose gel electrophoresis (Figure 2D1,D2) showed that the wtDps–AuNP mixture formed two separate bands, indicating the weak interaction between wtDps and AuNPs. Differently, the mixture of HBDps and AuNPs formed a smeared band with color overlap of AuNP in Figure 2D1c and the Coomassie brilliant blue (CBB) R-250 stained Dps in Figure 2D2c, indicative of the formation of the HBDps–AuNP complex originating from the high affinity of Ni^{2+}–NTA to Histag. This conclusion was further supported by the TEM observation that HBDps and AuNPs formed irregular aggregates (Figure 2E); in contrast, only isolated wtDps and AuNPs were observed (Figure 2F). The results of agarose gel electrophoresis and TEM consistently confirmed that the successful introduction of Histag onto the HBDps surface provides high affinity of HBDps to Ni^{2+}–NTA–AuNPs and further leads to the formation of Dps–AuNP nanoarchitectures (Figure 2E) via their interfacial interaction.

To construct mfDps, wtDps and HBDps were dissociated into monomers, mixed at 11:1 molar ratio of wtDps to HBDps, and reassembled. According to a random coassembly process, the 11:1 ratio would result in the highest yield of mfDps, and the reassembled product would contain 35.2% wtDps, 38.4% mfDps, and 26.4% Dps with more than one HBDps subunit (see Supporting Information for detailed analysis, Supporting Information Figure S2 and Table S1). MfDps can be purified from the mixture through nickel affinity chromatography (NAC). During the purification process, wtDps will be eliminated because of the absence of Histag on its external surface, and imidazole gradient elution can be used to separate mfDps from Dps containing more than one HBDps subunit per cage.

The coassembled product was first analyzed through size exclusion chromatography (SEC). As shown in Figure 3A, only a sharp peak around 13 mL appeared. TEM observation showed that there were dominantly 9 nm spheres like wtDps in the sample harvested from the peak (Figure 3B). SEC and TEM results together demonstrated that the mixed assembly of wtDps and HBDps subunits generated nanocage structures quite efficiently, without detectable monomers. After NAC, SDS-PAGE analysis of the contents of wtDps and HBDps in each fraction showed that a large amount of wtDps accompanying HBDps was eluted from the column by 150 mM imidazole after the 30 mM imidazole wash, suggesting the coassembly of wtDps and HBDps subunits. On the other hand, there was more HBDps than wtDps in the fraction of 500 mM imidazole, which implies that Dps species containing more than one HBDps subunits have higher affinity for the column and can be separated from mfDps under differential elution conditions (Figure 3C). To further reduce the content of Dps with more than one HBDps subunits in the final mfDps

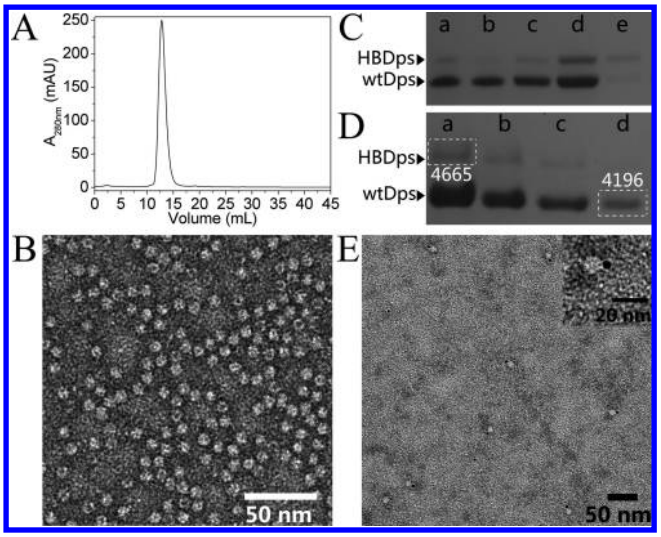

Figure 3. Characterization of mfDps. (A) SEC profile of the coassembled product of wtDps and HBDps subunits. (B) TEM image of the sample collected from the peak in part A. (C) SDS-PAGE analysis of different fractions in purification of mfDps via NAC. Lanes a–e, coassembly product of HBDps and wtDps, flowthrough, the fractions washed with 30, 150, and 500 mM imidazole, respectively. (D) Analysis of HBDps content in purified mfDps (elution with 100 mM imidazole) using SDS-PAGE/densitometry. Lanes a–d, the same mfDps sample with gradient loading volumes of 10, 5, 3, and 1 μL, respectively. Because band gray value is not linearly correlated to protein content among bands with quite different gray values, the two bands marked by dashed rectangles showed relatively equivalent gray values and were used for densitometry analysis. The numbers below the dashed rectangles correspond to the amount of protein in the marked band. Therefore, the molar ratio of wtDps to HBDps subunit can be calculated as $(4196/MW_{wtDps}/\text{loading volume}_{Lane\text{-}d})/(4665/MW_{HBDps}/\text{loading volume}_{Lane\text{-}a}) = (4196/18048.6/1)/(4665/21303.07/10) = 10.6$. (E) TEM image of mfDps–AuNP assembly with a 1:2 molar ratio of mfDps to AuNPs. Inset shows an enlarged view of the mfDps–AuNP complex.

preparation, 100 mM imidazole was used to elute the mfDps from the column for subsequent experiments. TEM examination showed that the sample in this fraction is dominantly the cage structure, and the molar ratio of wtDps subunit to HBDps subunit in the fraction was measured to be ca. 10.6:1 (Figure 3D). Therefore, the percentage of mfDps in this fraction, namely, the purity of mfDps, is estimated to be 96%. Furthermore, when mfDps was incubated with 3.5 nm Ni^{2+}–NTA–AuNPs, high yield of one Dps–one AuNP dimer structure was observed (Figure 3E). The result corroborated the success of monofunctionalization of Dps nanocage.

For a test of the monofunctionalization in controlling coassembly of Dps nanocages with AuNPs into discrete nanoarchitectures, mfDps was mixed with 13 nm Ni^{2+}–NTA–AuNPs with different stoichiometry. Native agarose gel electrophoresis was used to characterize the assembled products. After electrophoresis, the gel was imaged directly to record the mobility of AuNPs (Figure 4A1) and reimaged after staining with CBB R-250 to visualize the mfDps (Figure 4A2). As shown in Figure 4A1,A2, with the increase of molar ratio of mfDps to AuNPs, the mobility of AuNPs decreased, resulting in typical bands of different mobility. The result provided evidence that the interaction between mfDps and AuNPs occurred and implied that chimeras of AuNPs bound by specific numbers of mfDps might have formed. The

DOI: 10.1021/acsami.5b02823
ACS Appl. Mater. Interfaces 2015, 7, 11024–11031

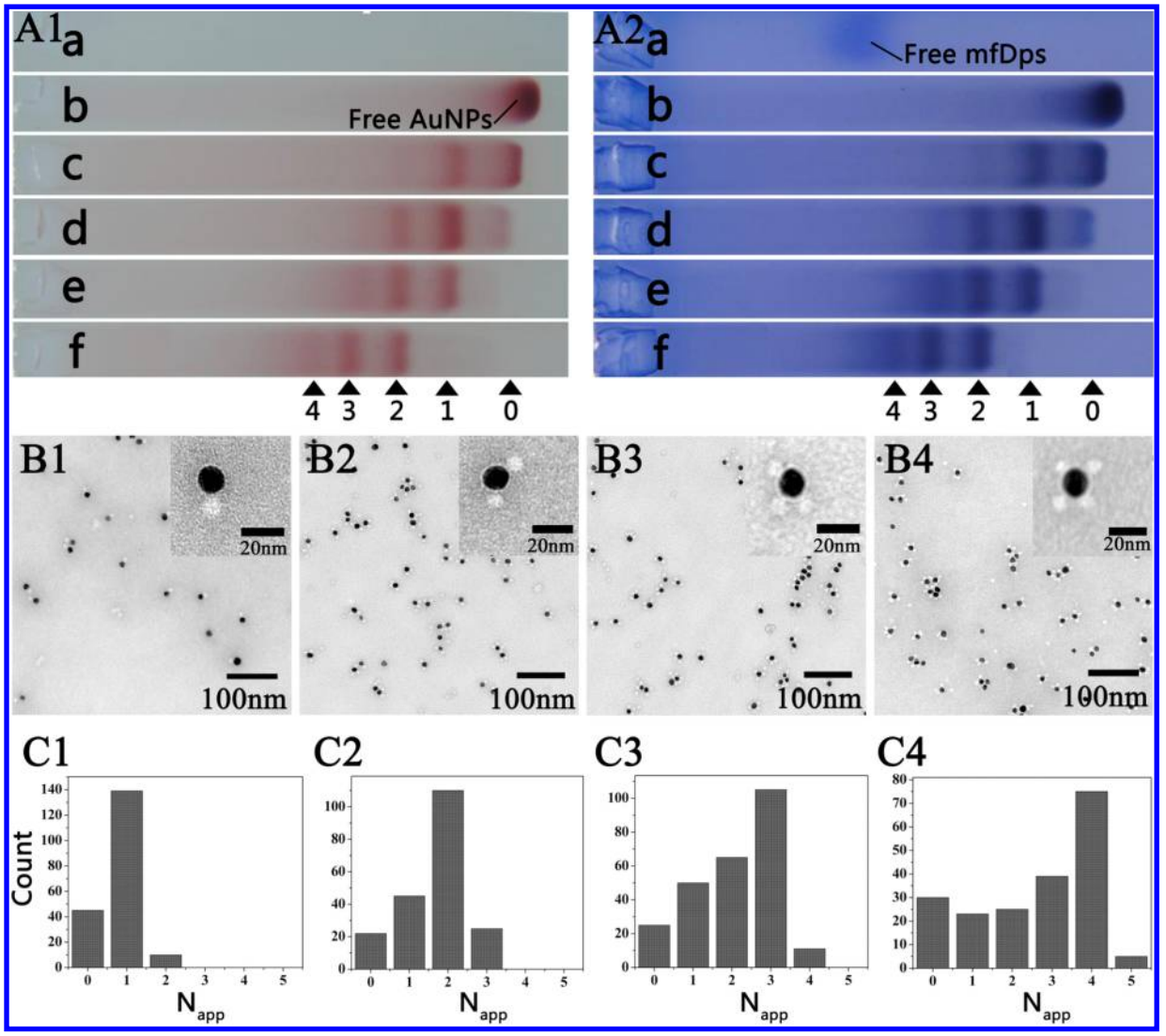

Figure 4. Assembly of mfDps on 13 nm AuNPs with variable stoichiometry. (A) Agarose gel (2.5%) electrophoresis of the coassembly products without (A1) and with (A2) CBB R-250 staining. Lane a, free mfDps; lane b, free 13 nm AuNPs; lanes c−f, coassembly products of AuNP and mfDps at molar ratios of 1:0.5, 1:1, 1:2, and 1:4, respectively. It is noted that, besides mfDps, free AuNPs were stained by CBB R-250, which is caused by incomplete destaining of the gel. Nevertheless, the result revealed that free mfDps had been separated from the AuNP-containing bands. Band 0 corresponds to free AuNPs, which was confirmed under TEM (data not shown). Bands 1−4 were subsequently found to be different complex architectures of mfDps−AuNPs under TEM. (B) TEM images of mfDps−AuNP nanoarchitectures recovered from bands 1−4 (corresponding to B1−B4, respectively) in the agarose gel. (C) The distribution of N_{app} of mfDps per AuNP in the mfDps−AuNP nanoarchitectures recovered from bands 1−4 (corresponding to C1−C4, respectively).

assembly products in different bands were purified and observed under TEM. Figure 4B1−B4 showed that mfDps and AuNPs formed well-organized hybrid structures, instead of uncontrollable large aggregates that were observed in the coassembly of HBDps and AuNPs (see Figure 2E). The mfDps appeared to be randomly distributed on AuNPs, which can be attributed to the isotropic modification of AuNPs by the Ni^{2+}−NTA chelates. The number of mfDps species per AuNP was counted, which is considered as an apparent one and herein is called N_{app}, because a small number of mfDps species may overlap with the associated AuNPs and thus may be invisible under TEM. Nevertheless, N_{app} can semiquantitatively reflect the abundance of mfDps on the AuNP surface. As shown in Figure 4C1−C4, N_{app} of each band showed a relatively narrow distribution, with peaks at 1, 2, 3, and 4 for bands 1, 2, 3, and 4, respectively. The slower the band migrated, the larger the N_{app} was. It is also noted that there were a few free AuNPs and mfDps species in all of these purified samples under TEM, indicating the dissociation of mfDps from AuNPs during sampling. More stable intermolecular binding strategies can be used to improve the stability in future fabrication of such kinds of hybrid structures. In addition, dynamic light scattering (DLS) measurement showed a gradual increase in the hydrodynamic diameter (HD) of the mfDps−AuNP architectures in samples from band 1 to band 4 (Supporting Information Figure S3), supporting the formation of a series of mfDps−AuNP architectures with the number of mfDps cages per AuNP tunable.

As demonstrated above, monofunctionalization of protein nanocages enables controllable assembly of hierarchical protein nanostructures by tuning the molar ratio of mfDps species to AuNPs. In addition, we can further assemble hierarchical Dps nanostructures by employing differently sized AuNPs as templates via the Ni^{2+}−Histag interaction between AuNPs

DOI: 10.1021/acsami.5b02823
ACS Appl. Mater. Interfaces 2015, 7, 11024−11031

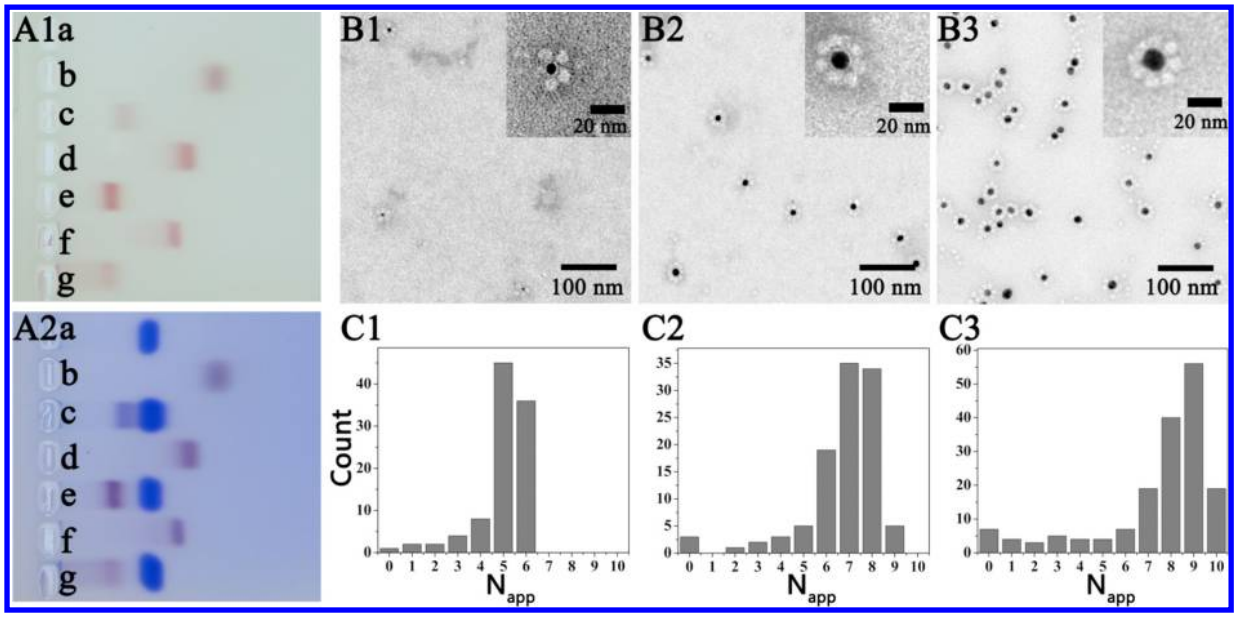

Figure 5. Assembly of mfDps on AuNPs with variable sizes at excessive ratios of mfDps to AuNPs. (A) Agarose gel (3%) electrophoresis of the coassembly products without (A1) and with (A2) CBB R-250 staining. Lane a, free mfDps; lanes b, d, and f, free AuNPs of 5, 10, and 13 nm, respectively; lanes c, e, and g, coassembly products of mfDps with AuNPs of 5, 10, and 13 nm, respectively. (B) TEM images of mfDps−AuNP assembly products, in which the AuNP sizes are 5 nm (B1), 10 nm (B2), and 13 nm (B3), respectively. (C) The distribution of N_{app} of mfDps per AuNP in the mfDps−AuNP nanoarchitectures, in which the AuNP sizes are 5 nm (C1), 10 nm (C2), and 13 nm (C3), respectively.

and mfDps. In this study, AuNPs with diameters of 5, 10, and 13 nm were applied as the templates, and they were theoretically estimated to be able to accommodate at most 8, 16, and 22 Dps per AuNP, respectively (see Supporting Information for detailed analysis, Figure S5). An excessive amount of mfDps was mixed with AuNPs of various sizes to maximize the number of mfDps species bound on the AuNP surface. Analysis by agarose gel electrophoresis showed that incubation with excessive mfDps resulted in a single band with much slower mobility in comparison with free AuNPs in all the cases of AuNPs of the three different diameters, implying that relatively homogeneous assemblies probably formed (Figure 5A1). CBB R-250 staining of the gel showed that unbound mfDps can be separated from the AuNP-containing band (Figure 5A2). TEM observation of the coassembly products recovered from the gel band showed that mfDps bound to AuNPs of the three different diameters efficiently, resulting in flower-like structures under the 2D projection of TEM with AuNPs as pistil and mfDps as petal (Figure 5B1−B3). Distributions of N_{app} were obtained by analyzing about 100 clusters for each size of AuNPs (Figure 5C1−C3). As the AuNP size increased, N_{app} became larger and peaked at 5, 7, and 9 in clusters templated by AuNPs of 5, 10, and 13 nm, respectively. Further analysis of the recovered samples by DLS revealed that the HDs of mfDps−AuNP architectures peaked at 27.85, 32.61, and 34.94 nm for AuNP templates of 5, 10, and 13 nm, respectively (Supporting Information Figure S4). The increasing tendency of mfDps−AuNP architecture size, as the AuNP size became larger, supported the formation of superstructures of mfDps cages templated by differently sized AuNPs. These results demonstrate that the feasibility of precise assembly of protein architectures through surface monofunctionalization, together with the introduction of variable size templates.

The well-known interaction between Histag and Ni^{2+}−NTA has been utilized to construct protein−AuNP complexes. Without rational design and selective gene fusion of the Histag on specific site, this strategy merely works well in hierarchical assembly of discrete protein nanoarchitectures when the sites for Histag introduction are highly localized, in rare cases. For example, Hu et al. fused Histag to the N terminus of an adenovirus serotype 12 knob, a trimeric protein. Because the three Histags happened to be localized on the same side of the knob, dimers, trimers, and shells of knob were successfully assembled on Ni^{2+}−NTA−AuNPs.[25] However, in many more cases, because protein nanostructures (e.g., ferritins, viral NPs, etc.) in nature are highly symmetric, which results in symmetric distribution of fused Histags on them, the application of this strategy often leads to formation of infinite arrays or agglomeration due to the lack of spatial control over the binding sites. A typical example also comes from the work by Hu et al. mentioned above, in which the coassembly of AuNPs with a *Mycobacterium tuberculosis* 20S proteasome using the same strategy just generated 2D protein arrays, rather than discrete nanoarchitectures.[25] It is notable that the strategy described in this contribution, i.e., monofunctionalization of Dps by introducing a single Histag onto the Dps nanocage, has proven to be an effective way to spatially control the assembly of discrete protein nanoarchitectures by precisely engineering the monovalent protein−NP interaction.

Controllable assembly of nanomaterials has been a hot topic in nanoscience.[26−29] In particular, coassembly of biomacromolecules and chemically synthesized nanomaterials enables integration of the advantages of different types of building blocks. The architectures of Dps protein nanocages together with AuNPs assembled above may represent a new kind of multifunctional platform. On one hand, protein nanocages possess interesting structural and biochemical properties in terms of self-assembly, symmetry, addressability, functionalization, and environmental response,[30,31] and have shown potential for various purposes such as cargo encapsulation and delivery,[32−36] nanotemplates,[37−39] nanoreactors,[40,41] and

DOI: 10.1021/acsami.5b02823
ACS Appl. Mater. Interfaces 2015, 7, 11024−11031

sensing.[42−44] Further assembly of these biological nanomaterials into hierarchical architectures is intriguing with respect to rational organization of nanoreactors or nanocontainers as well as module development for synthetic biology. On the other hand, the chemically synthesized nanomaterials, which often possess unique chemical and physical properties, such as catalytic, optical, magnetic, or electronic features, would endow the complicated protein architectures with extra performance. It can be envisioned that designed assembly of protein nanostructures into higher-order finite architectures with chemically synthesized nanomaterials in a controllable manner will open new opportunities for integrated materials and devices with unprecedented features.

3. CONCLUSION

In this work, we have successfully demonstrated a facile strategy to precisely fabricate organic−inorganic hybrid architectures with protein nanostructure as the building block using AuNPs as scaffolds. The rationally designed specific interaction between the protein nanostructure and AuNPs guides the self-assembly of hierarchical nanoarchitectures. That is, AuNP surface was comprehensively modified with Ni^{2+}−NTA chelates, while each Dps cage was installed with only one Histag on the external surface. Such surface monofuctionalization is an important prerequisite for assembly of discrete hierarchical protein architectures as well as the fine-tunability thereof. The protein nanocages surrounding the metal NP, in future, can be filled with various materials including magnetic NPs, dyes, enzymes, drugs, etc.,[30] while the scaffold NPs can contribute additional physical or chemical properties. Therefore, the architectures generated here hold great potential as a novel platform for investigation of synergetic effects at the nanometer scale and functionality integration as well. The method described here for assembling finite protein superstructures through finely engineering a protein−metal NP interface can be extended to other protein nanostructures and be borrowed by synthetic biology for biomacromolecules manipulation.

4. EXPERIMENTAL SECTION

Synthesis of 3.5, 5, 10, and 13 nm AuNPs and Surface Modification. The synthesis of 3.5 and 5 nm AuNPs follows the methods of Nikhil R. Jana[45] and Handley,[46] respectively. A general seeded growth route was used to synthesize large, monodisperse citrate-stabilized 10 nm AuNPs through kinetic control of the reaction conditions as described previously.[47] AuNPs of 13 nm in diameter were synthesized following Fern's method.[48] All AuNPs were characterized with TEM and UV−vis spectroscopy.

Surface functionalization of AuNPs with Ni^{2+}−NTA was carried out as follows. For functionalization of 13 nm AuNPs, AuNPs, Dithiobis(C2-NTA), and Ni(II) were successively mixed in the ratio of 1:3200:3000. In detail, Dithiobis(C2-NTA) solution (0.172 mL, 2.6 mM) was added to 13 nm AuNPs solution (10 mL, 14 nM). After the mixture was shaken for 15 min, 250 mM Tris-HCl, pH 8.0 (1.13 mL) was added, followed by stirring at room temperature for 12 h. Then, the mixture was dialyzed against 25 mM Tris-HCl, pH 8.0, using 8−14 kDa cutoff membrane to remove excess Dithiobis(C2-NTA) and was added with $NiSO_4$ solution (8.4 μL, 50 mM) under stirring. Fifteen minutes later, excess $NiSO_4$ was removed by dialysis under the same condition as above. Finally, the 13 nm Ni^{2+}−NTA−AuNPs were enriched to 3 mL through osmotic ultrafiltration against polyethylene glycol 20 000.

The functionalization of 3.5, 5, and 10 nm AuNPs was performed similarly except that AuNPs, Dithiobis(C2-NTA), and $NiSO_4$ were mixed in ratios of 1:400:3000, 1:800:3000, and 1:1600:3000 for 3.5, 5, and 10 nm AuNPs, respectively.

Construction and Preparation of wtDps and HBDps. The coding sequence of wtDps was synthesized and cloned into the pET32a plasmid between Nde I and Xho I restriction sites, resulting in the expression vector pET32a-wtDps. The plasmid was transformed into the *E. coli* BL21 (DE3) strain. The expression of wtDps was induced with the addition of 1 mM isopropyl-β-D-thiogalactopyranoside (IPTG) when the culture OD_{600} reached 0.6. The extraction and purification of recombinant wtDps protein was carried out as previously described.[49]

A short peptide (MGSHHHHHHGSGLNDIFEAQKIEWHEGGS) containing a Histag and a spacer was genetically fused to the N-terminus of wtDps by three rounds of PCR with pET32a-wtDps as template, using upstream primers: 5′ CGCAGAAAATCGAATGGCATGAAGGTGGCTCAATGAAAACAATCAACTCAGT 3′ (first round), 5′ CCATGGTTCAGGCCTGAACGACATCTTCGAAGCGCAGAAAATCGAATGGCAT 3′ (second round), 5′ GGAATTCCATATGGGCTCGCACCATCACCATCACCATGGTTCAGGCCTGAACG 3′ (third round), and a common downstream primer 5′ GCTTCCTTTCGGGCTTTGTTAG 3′. The resultant coding sequence (HBDps) was cloned into pET32a plasmid between Nde I and Xho I restriction sites, resulting in the expression vector pET32a-HBDps. Recombinant expression of HBDps was carried out as that of wtDps. Purification of HBDps by NAC was performed with the HisTrap FF column according to the manufacturer's instructions. Protein concentration was determined using the Bradford assay.

Surface Monofuctionalization of Dps Cages. WtDps (3 mL, 8 mg/mL), HBDps (0.35 mL, 6.3 mg/mL), and 18 mL buffer (50 mM Tris-HCl, pH 8.0, 0.5 M NaCl) were mixed equally with the molar ratio of wtDps to HBDps being 11:1 and then dialyzed against water, the pH of which was gradually reduced to 2.0 to dissociate wtDps and HBDps cages into subunits by adding 100 mM HCl using a syringe pump. After further dialysis against the solution of pH 2.0 at 4 °C overnight, the mixture of HBDps and wtDps was allowed to reassemble by a gradual increase of the pH. In detail, the dialysis tubing of mixed subunits was placed into 1 mM phosphate buffer at pH 2.0. The pH was raised to pH 7.0 by gradually adding 2 M NaOH using a syringe pump, and the sample was dialyzed at 4 °C overnight. Afterward, the sample was loaded into a nickel affinity column which was subsequently washed with 5 and 25 mM imidazole to eliminate any Dps formed from mere wtDps. The mfDps was eluted from the column with 100 mM imidazole. Negative-staining TEM was used to characterize the structural integrity of the asprepared mfDps. SDS-PAGE and densitometry were used to analyze the contents of wtDps and HBDps in the asprepared mfDps.

Coassembly of AuNPs with Protein Nanocages. HBDps, wtDps, or mfDps was mixed with Ni^{2+}−NTA−AuNPs of a certain diameter at molar ratios as indicated in 25 mM Tris-HCl, pH 7.4. The mixtures were shaken at 1000 rpm at 4 °C overnight to allow adequate interactions between Dps and AuNPs. The coassembly products were characterized with native agarose gel electrophoresis and TEM. Different populations in the coassembly products can be separated in electrophoresis. Bands of interest were excised from the gel, recovered through electroelution, and subjected to TEM characterization.

Agarose Gel Electrophoresis. Samples were mixed well with one-fifth volume of 15% ficoll and loaded into agarose gels in running buffer (25 mM Tris−HAc, pH 7.4). Electrophoresis was run for 50 min at 100 V with the chamber in an ice bath. The gels were imaged immediately after electrophoresis. For visualizing protein, the gels were first stained with CBB R-250 and then reimaged.

Transmission Electron Microscopy. A sample (20 μL) was deposited onto a carbon coated copper grid and was blotted off with filter paper after 5 min. Samples containing Dps protein were further negatively stained with 2% phosphotungstate for 2 min. All samples were observed under a FEI Tecnai 20 TEM (operated at 200 kV) equipped with a Gatan UltraScan 894 CCD camera. TEM images were processed using the ImageJ software.

Dynamic Light Scattering. DLS measurement was performed on a zetasizer Nano ZS (Malvern) as previously described.[50]

DOI: 10.1021/acsami.5b02823
ACS Appl. Mater. Interfaces 2015, 7, 11024−11031

■ ASSOCIATED CONTENT

Supporting Information

Additional figures, table, and calculation. The Supporting Information is available free of charge on the ACS Publications website at DOI: 10.1021/acsami.5b02823.

■ AUTHOR INFORMATION

Corresponding Authors

*E-mail: fli@wh.iov.cn.

*E-mail: qbwang2008@sinano.ac.cn.

Notes

The authors declare no competing financial interest.

■ ACKNOWLEDGMENTS

F.L. acknowledges funding by NSFC (Grant No. 31271076) and the Key Research Program of the Chinese Academy of Sciences (Grant No. KGZD-EW-T02-3). Q.W. acknowledges funding by Chinese Academy of Sciences "Strategic Priority Research Program" (Grant No. XDA01030200), the Chinese Ministry of Science and Technology (Grant No. 2011CB965004), the National Science Foundation of China (Grant No. 21303249, 21425103, 21473240), and the National Science Foundation of Jiangsu province, China (Grant No. BK2012007).

■ REFERENCES

(1) Abrahams, J. P.; Leslie, A. G. W.; Lutter, R.; Walker, J. E. Structure at 2.8-Angstrom Resolution of F1-ATPase from Bovine Heart-Mitochondria. *Nature* **1994**, *370*, 621−628.

(2) Mitchison, T.; Kirschner, M. Microtubule Assembly Nucleated by Isolated Centrosomes. *Nature* **1984**, *312*, 232−237.

(3) Kerfeld, C. A.; Sawaya, M. R.; Tanaka, S.; Nguyen, C. V.; Phillips, M.; Beeby, M.; Yeates, T. O. Protein Structures Forming the Shell of Primitive Bacterial Organelles. *Science* **2005**, *309*, 936−938.

(4) Yang, R.; Chen, L.; Yang, S.; Lv, C.; Leng, X.; Zhao, G. 2D Square Arrays of Protein Nanocages through Channel-Directed Electrostatic Interactions with Poly(Alpha, L-Lysine). *Chem. Commun.* **2014**, *50*, 2879−2882.

(5) Luo, Q.; Dong, Z.; Hou, C.; Liu, J. Protein-Based Supramolecular Polymers: Progress and Prospect. *Chem. Commun.* **2014**, *50*, 9997−10007.

(6) King, N. P.; Bale, J. B.; Sheffler, W.; McNamara, D. E.; Gonen, S.; Gonen, T.; Yeates, T. O.; Baker, D. Accurate Design of Co-assembling Multi-component Protein Nanomaterials. *Nature* **2014**, *510*, 103−108.

(7) Cespedes, M. V.; Unzueta, U.; Tatkiewicz, W.; Sanchez-Chardi, A.; Conchillo-Sole, O.; Alamo, P.; Xu, Z. K.; Casanova, I.; Corchero, J. L.; Pesarrodona, M.; Cedano, J.; Daura, X.; Ratera, I.; Veciana, J.; Ferrer-Miralles, N.; Vazquez, E.; Villaverde, A.; Mangues, R. In Vivo Architectonic Stability of Fully *De Novo* Designed Protein-Only Nanoparticles. *ACS Nano* **2014**, *8*, 4166−4176.

(8) Sinclair, J. C. Constructing Arrays of Proteins. *Curr. Opin. Chem. Biol.* **2013**, *17*, 946−951.

(9) Kostiainen, M. A.; Hiekkataipale, P.; Laiho, A.; Lemieux, V.; Seitsonen, J.; Ruokolainen, J.; Ceci, P. Electrostatic Assembly of Binary Nanoparticle Superlattices Using Protein Cages. *Nat. Nanotechnol.* **2013**, *8*, 52−56.

(10) King, N. P.; Sheffler, W.; Sawaya, M. R.; Vollmar, B. S.; Sumida, J. P.; Andre, I.; Gonen, T.; Yeates, T. O.; Baker, D. Computational Design of Self-assembling Protein Nanomaterials with Atomic Level Accuracy. *Science* **2012**, *336*, 1171−1174.

(11) Brodin, J. D.; Ambroggio, X. I.; Tang, C.; Parent, K. N.; Baker, T. S.; Tezcan, F. A. Metal-Directed, Chemically Tunable Assembly of One-, Two- and Three-Dimensional Crystalline Protein Arrays. *Nat. Chem.* **2012**, *4*, 375−382.

(12) Lai, Y. T.; Cascio, D.; Yeates, T. O. Structure of A 16-nm Cage Designed by Using Protein Oligomers. *Science* **2012**, *336*, 1129−1129.

(13) Lai, Y. T.; Tsai, K. L.; Sawaya, M. R.; Asturias, F. J.; Yeates, T. O. Structure and Flexibility of Nanoscale Protein Cages Designed by Symmetric Self-Assembly. *J. Am. Chem. Soc.* **2013**, *135*, 7738−7743.

(14) Fletcher, J. M.; Harniman, R. L.; Barnes, F. R.; Boyle, A. L.; Collins, A.; Mantell, J.; Sharp, T. H.; Antognozzi, M.; Booth, P. J.; Linden, N.; Miles, M. J.; Sessions, R. B.; Verkade, P.; Woolfson, D. N. Self-Assembling Cages from Coiled-Coil Peptide Modules. *Science* **2013**, *340*, 595−599.

(15) Przybyla, D. E.; Perez, C. M. R.; Gleaton, J.; Nandwana, V.; Chmielewski, J. Hierarchical Assembly of Collagen Peptide Triple Helices into Curved Disks and Metal Ion-Promoted Hollow Spheres. *J. Am. Chem. Soc.* **2013**, *135*, 3418−3422.

(16) Jiang, T.; Xu, C. F.; Liu, Y.; Liu, Z.; Wall, J. S.; Zuo, X. B.; Lian, T. Q.; Salaita, K.; Ni, C. Y.; Pochan, D.; Conticello, V. P. Structurally Defined Nanoscale Sheets from Self-Assembly of Collagen-Mimetic Peptides. *J. Am. Chem. Soc.* **2014**, *136*, 4300−4308.

(17) Sinclair, J. C.; Davies, K. M.; Venien-Bryan, C.; Noble, M. E. Generation of Protein Lattices by Fusing Proteins with Matching Rotational Symmetry. *Nat. Nanotechnol.* **2011**, *6*, 558−562.

(18) Klem, M. T.; Willits, D.; Young, M.; Douglas, T. 2-D Array Formation of Genetically Engineered Viral Cages on Au Surfaces and Imaging by Atomic Force Microscopy. *J. Am. Chem. Soc.* **2003**, *125*, 10806−10807.

(19) Sperling, R. A.; Parak, W. J. Surface Modification, Functionalization and Bioconjugation of Colloidal Inorganic Nanoparticles. *Philos. Trans. R. Soc., A* **2010**, *368*, 1333−1383.

(20) Zhang, T.; Dong, Y.; Sun, Y.; Chen, P.; Yang, Y.; Zhou, C.; Xu, L.; Yang, Z.; Liu, D. DNA Bimodified Gold Nanoparticles. *Langmuir* **2012**, *28*, 1966−1970.

(21) Zhang, T.; Yang, Z.; Liu, D. DNA Discrete Modified Gold Nanoparticles. *Nanoscale* **2011**, *3*, 4015−4021.

(22) Li, F.; Chen, Y. H.; Chen, H. L.; He, W.; Zhang, Z. P.; Zhang, X. E.; Wang, Q. B. Monofunctionalization of Protein Nanocages. *J. Am. Chem. Soc.* **2011**, *133*, 20040−20043.

(23) Ilari, A.; Stefanini, S.; Chiancone, E.; Tsernoglou, D. The Dodecameric Ferritin from *Listeria Innocua* Contains A Novel Intersubunit Iron-Binding Site. *Nat. Struct. Biol.* **2000**, *7*, 38−43.

(24) Kang, S.; Oltrogge, L. M.; Broomell, C. C.; Liepold, L. O.; Prevelige, P. E.; Young, M.; Douglas, T. Controlled Assembly of Bifunctional Chimeric Protein Cages and Composition Analysis Using Noncovalent Mass Spectrometry. *J. Am. Chem. Soc.* **2008**, *130*, 16527−16529.

(25) Hu, M. H.; Qian, L. P.; Brinas, R. P.; Lymar, E. S.; Hainfeld, J. F. Assembly of Nanoparticle-Protein Binding Complexes: From Monomers to Ordered Arrays. *Angew. Chem., Int. Ed.* **2007**, *46*, 5111−5114.

(26) Jones, M. R.; Osberg, K. D.; Macfarlane, R. J.; Langille, M. R.; Mirkin, C. A. Templated Techniques for the Synthesis and Assembly of Plasmonic Nanostructures. *Chem. Rev.* **2011**, *111*, 3736−3827.

(27) Schreiber, R.; Do, J.; Roller, E. M.; Zhang, T.; Schuller, V. J.; Nickels, P. C.; Feldmann, J.; Liedl, T. Hierarchical Assembly of Metal Nanoparticles, Quantum Dots and Organic Dyes Using DNA Origami Scaffolds. *Nat. Nanotechnol.* **2014**, *9*, 74−78.

(28) Do, J.; Schreiber, R.; Lutich, A. A.; Liedl, T.; Rodriguez-Fernandez, J.; Feldmann, J. Design and Optical Trapping of A Biocompatible Propeller-Like Nanoscale Hybrid. *Nano Lett.* **2012**, *12*, 5008−5013.

(29) Yan, J.; Hu, C. Y.; Wang, P.; Zhao, B.; Ouyang, X. Y.; Zhou, J.; Liu, R.; He, D. N.; Fan, C. H.; Song, S. P. Growth and Origami Folding of DNA on Nanoparticles for High-Efficiency Molecular Transport in Cellular Imaging and Drug Delivery. *Angew. Chem., Int. Ed.* **2015**, *54*, 2431−2435.

(30) Li, F.; Wang, Q. B. Fabrication of Nanoarchitectures Templated by Virus-Based Nanoparticles: Strategies and Applications. *Small* **2014**, *10*, 230−245.

(31) Uchida, M.; Klem, M. T.; Allen, M.; Suci, P.; Flenniken, M.; Gillitzer, E.; Varpness, Z.; Liepold, L. O.; Young, M.; Douglas, T. Biological Containers: Protein Cages as Multifunctional Nanoplatforms. *Adv. Mater.* **2007**, *19*, 1025−1042.

DOI: 10.1021/acsami.5b02823
ACS Appl. Mater. Interfaces 2015, 7, 11024−11031

(32) Dixit, S. K.; Goicochea, N. L.; Daniel, M. C.; Murali, A.; Bronstein, L.; De, M.; Stein, B.; Rotello, V. M.; Kao, C. C.; Dragnea, B. Quantum Dot Encapsulation in Viral Capsids. *Nano Lett.* **2006**, *6*, 1993−1999.
(33) Loo, L.; Guenther, R. H.; Lommel, S. A.; Franzen, S. Encapsidation of Nanoparticles by Red Clover Necrotic Mosaic Virus. *J. Am. Chem. Soc.* **2007**, *129*, 11111−11117.
(34) Li, F.; Zhang, Z. P.; Peng, J.; Cui, Z. Q.; Pang, D. W.; Li, K.; Wei, H. P.; Zhou, Y. F.; Wen, J. K.; Zhang, X. E. Imaging Viral Behavior in Mammalian Cells with Self-Assembled Capsid-Quantum-Dot Hybrid Particles. *Small* **2009**, *5*, 718−726.
(35) Molino, N. M.; Wang, S. W. Caged Protein Nanoparticles for Drug Delivery. *Curr. Opin. Biotechnol.* **2014**, *28*, 75−82.
(36) Zeng, Q. B.; Wen, H. B.; Wen, Q.; Chen, X. H.; Wang, Y. G.; Xuan, W. L.; Liang, J. S.; Wan, S. H. Cucumber Mosaic Virus as Drug Delivery Vehicle for Doxorubicin. *Biomaterials* **2013**, *34*, 4632−4642.
(37) Wang, Q.; Lin, T. W.; Tang, L.; Johnson, J. E.; Finn, M. G. Icosahedral Virus Particles as Addressable Nanoscale Building Blocks. *Angew. Chem., Int. Ed.* **2002**, *41*, 459−462.
(38) Li, F.; Gao, D.; Zhai, X. M.; Chen, Y. H.; Fu, T.; Wu, D. M.; Zhang, Z. P.; Zhang, X. E.; Wang, Q. B. Tunable, Discrete, Three-Dimensional Hybrid Nanoarchitectures. *Angew. Chem., Int. Ed.* **2011**, *50*, 4202−4205.
(39) Capehart, S. L.; Coyle, M. P.; Glasgow, J. E.; Francis, M. B. Controlled Integration of Gold Nanoparticles and Organic Fluorophores Using Synthetically Modified MS2 Viral Capsids. *J. Am. Chem. Soc.* **2013**, *135*, 3011−3016.
(40) Comellas-Aragones, M.; Engelkamp, H.; Claessen, V. I.; Sommerdijk, N. A.; Rowan, A. E.; Christianen, P. C.; Maan, J. C.; Verduin, B. J.; Cornelissen, J. J.; Nolte, R. J. A Virus-Based Single-Enzyme Nanoreactor. *Nat. Nanotechnol.* **2007**, *2*, 635−639.
(41) Douglas, T.; Young, M. Host-Guest Encapsulation of Materials by Assembled Virus Protein Cages. *Nature* **1998**, *393*, 152−155.
(42) Huang, P.; Rong, P.; Jin, A.; Yan, X.; Zhang, M. G.; Lin, J.; Hu, H.; Wang, Z.; Yue, X.; Li, W.; Niu, G.; Zeng, W.; Wang, W.; Zhou, K.; Chen, X. Dye-Loaded Ferritin Nanocages for Multimodal Imaging and Photothermal Therapy. *Adv. Mater.* **2014**, *26*, 6401−6408.
(43) Meldrum, T.; Seim, K. L.; Bajaj, V. S.; Palaniappan, K. K.; Wu, W.; Francis, M. B.; Wemmer, D. E.; Pines, A. A Xenon-Based Molecular Sensor Assembled on an MS2 Viral Capsid Scaffold. *J. Am. Chem. Soc.* **2010**, *132*, 5936−5937.
(44) Qazi, S.; Liepold, L. O.; Abedin, M. J.; Johnson, B.; Prevelige, P.; Frank, J. A.; Douglas, T. P22 Viral Capsids as Nanocomposite High-Relaxivity MRI Contrast Agents. *Mol. Pharmaceutics* **2013**, *10*, 11−17.
(45) Jana, N. R.; Gearheart, L.; Murphy, C. J. Seeding Growth for Size Control of 5−40 nm Diameter Gold Nanoparticles. *Langmuir* **2001**, *17*, 6782−6786.
(46) Handley, D. A. *Colloidal Gold: Principles, Methods and Applications*; Hayat, M. A., Ed.; Academic Press: New York, 1989; Vol. *1*, pp 13−32.
(47) Bastus, N. G.; Comenge, J.; Puntes, V. Kinetically Controlled Seeded Growth Synthesis of Citrate-Stabilized Gold Nanoparticles of up to 200 nm: Size Focusing versus Ostwald Ripening. *Langmuir* **2011**, *27*, 11098−11105.
(48) Frens, G. Controlled Nucleation for the Regulation of the Particlesize in Monodisperse Gold Solutions. *Nat. Med.* **1973**, *241*, 20−22.
(49) Allen, M.; Willits, D.; Mosolf, J.; Young, M.; Douglas, T. Protein Cage Constrained Synthesis of Ferrimagnetic Iron Oxide Nanoparticles. *Adv. Mater.* **2002**, *14*, 1562−1565.
(50) Li, F.; Chen, H. L.; Zhang, Y. J.; Chen, Z.; Zhang, Z. P.; Zhang, X. E.; Wang, Q. B. Three-Dimensional Gold Nanoparticle Clusters with Tunable Cores Templated by A Viral Protein Scaffold. *Small* **2012**, *8*, 3832−3838.

DOI: 10.1021/acsami.5b02823
ACS Appl. Mater. Interfaces 2015, 7, 11024−11031